RAMAN GAIN AND STRUCTURAL OF TELLURITE-PHOSPHATE GLASSES WITH DIFFERENT MODIFIERS DOPING WITH Er_2O_3

H. A. OTHMAN[a], M. M. ALQAHTANI[b], M. REBEN[c], EL S. YOUSEF[b,d,*]
[a]Physics Department, Faculty of Science, Menoufa University, Shebin El-Koom, Menoufa 32511, Egypt.
[b]Department of Physics, Faculty of Science, King Khalid University, P.O. Box 9004, Post. Code: 61421, Abha, Saudi Arabia.
[c]Faculty of Materials Science and Ceramics, AGH – University of Science and Technology, al. Mickiewicza 30, 30-059 Cracow, Poland.
[d]Faculty of Science, Physics Department, Al Azhar University, Assiut branch, Assiut, Egypt.

A glass series of Te-glasses ($70TeO_2$- $10P_2O_5$- $10ZnO$- $5PbF_2$) modified with 5mol % of different modifiers (WO_3, Al_2O_3, CdO, SrO, BaO), that was then doped with 600ppm Er_2O_3 was prepared by melt quench technique. The effect of modifier oxide on the Te-glass structure was studied using Raman spectroscopy. The Obtained Raman spectra reveal the characteristic structural units TeO_4 and TeO_3. Er_2O_3 doping along with the type of oxide modifier influenced the tellurite glass network and hence the Raman spectral features. The change in the Boson peak features depend on the rare earth ion doping. The obtained Raman spectra were deconvoluted to follow the structural changes. The deconvoluted data show a transformation of TeO_4 to TeO_3 upon the addition of metal oxides. Due to the higher coordination of WO_3 and Al_2O_3 that offers more oxygens when compared with alkaline modifiers, the TeO_3 structural group is dominated. Raman gain was calculated for the prepared glasses. Al_2O_3 modified glass sample has the highest Raman gain.

1. Introduction

Compared to phosphate and Silicate glasses, tellurium dioxide based glasses have great interest due to their physical and chemical properties such as low phonon energy ($640–790cm^{-1}$) vibration bands for the trigonal pyramid, bipyramid and polyhedral that makes them attractive for designing of Raman amplifiers, sensors, switching devices, near-IR and mid-IR lasers [1- 3], Beside their low melting temperature, good solubility of rare-earth ions and large thermo-optic coefficient, tellurium glasses also characterized by high refractive index, high dielectric constant, wide infrared transparency and excellent third-order nonlinear optical properties [4- 7]. Adding fluorides such as PbF_2, BaF_2, LiF, ZnF_2…etc, to glass matrix lower the non-radiative decay rates and improve the emission efficiency [8-10]. The glass-forming ability of tellurite glasses enhances by adding modifiers such as transition metal, alkali, alkaline-earth and rare earth metal oxides [11] and modify the main structural units TeO_4 and TeO_3 of Tellurite glasses. The addition of alkaline earth oxides such as BaO and SrO increases the thermal stability of the glasses [12, 13]. Also, heavy metal oxides (ZnO, PbO and CdO) based glasses have a wide range of applications in the field of optical and electronic devices [14, 15]. Chemical and thermal stability of tellurite glass increase with the addition of Al_2O_3 that lead also to the transformation: $TeO_4 \rightarrow TeO_3$ [16, 13]. Also adding Al_2O_3 to the RE doped glass matrix enhance the dispersion of rare earth in glasses, helping to limit the concentration quenching of the photoluminescence features [17]. Addition of WO_3 into TeO_2 results in the formation of W–O–W and Te–O–W linkages. The formation of Te–O–W bridging bonds increases the connectivity of the network and stabilizes the glass formation.

---

* Corresponding author: omn_yousef2000@yahoo.com

It also leads to increasing lower co-ordination units TeO_3/TeO_{3+1} at the expense of higher coordination TeO_4 units in the glass network [18]. The addition of WO_3 leads to good electrochromic and photochromic properties so it could be widely used in electrochromic, optical modulation and solar energy [19]. Besides their high rare-earth solubility, tellurite glasses also prevent erbium clustering and luminescence quenching, so Er-doped tellurite glasses exhibit a broad emission at 1.53 μm with a high quantum efficiency [20-23]. Tellurium glasses doped with Er^{3+} are good candidates for applications such as optical amplifiers, laser light modulators and fibre lasers [24, 25]. Dousti et al. reported that the up-conversion process is enhanced in zinc tellurite glass doped with Er^{3+} ion [26]. Raman gain has received great interest because it considered as a mean for all-optical amplification processes [27]. TeO2 glasses are characterized by their high Raman gain when compared with SiO2 glasses [28]. Erbium-doped P2O5-tellurite glasses are a good candidate for waveguide amplifiers at λ=1.5 μm [29].

The aim of this paper is to investigate the effect of different modifier oxides with different coordination on the structure and Raman gain of undoped $70TeO_2$- $10P_2O_5$- $10ZnO$- $5PbF_2$ glasses and when doped with Er_2O_3.

2. Experimental

The glasses with the composition ($70TeO_2$- $10P_2O_5$- $10ZnO$- $5PbF_2$) modified with 5mol % of different modifiers (WO_3, Al_2O_3, CdO, SrO, BaO) by using melt- quenching method, that was then doped with 600ppm Er_2O_3. Where the composition $70TeO_2$–$5WO_3$–$10P_2O_5$–$10ZnO$–$5PbF_2$ (label W), $70TeO_2$–$5WO_3$–$10P_2O_5$–$10ZnO$–$5PbF_2$+ 600ppm Er_2O_3 (Label W-Er), $70TeO_2$–$5CdO$–$10P_2O_5$–$10ZnO$–$5PbF_2$ (Label Cd), $70TeO_2$–$5CdO$–$10P_2O_5$–$10ZnO$–$5PbF_2$+600ppm Er_2O_3 (Label Cd-Er), $70TeO_2$–$5Al_2O_3$–$10P_2O_5$–$10ZnO$–$5PbF_2$ (Label Al), $70TeO_2$–$5Al_2O_3$–$10P_2O_5$–$10ZnO$–$5PbF_2$ + 600ppm Er_2O_3 (Label Al-Er), $70TeO_2$–$5SrO$–$10P_2O_5$–$10ZnO$–$5PbF_2$ (Label Sr), $70TeO_2$–$5SrO$–$10P_2O_5$–$10ZnO$–$5PbF_2$ + 600ppm Er_2O_3 (Label Sr-Er), $70TeO_2$–$5BaO$–$10P_2O_5$–$10ZnO$–$5PbF_2$ (Label Ba), and $70TeO_2$–$5BaO$–$10P_2O_5$–$10ZnO$–$5PbF_2$ (Label Ba-Er). The Spontaneous Raman spectra of the prepared glass which are vertically (VV) polarized were acquired using Thermo Scientific DXR Raman Microscope Spectroscopy setup with 532nm excitation [532nm Laser type Diode-pumped, solid state (DPSS)]. The V-polarized Raman scattered signal was collected in the backscattering geometry with a 100× microscope objective.

3. Results and discussion

Raman spectra of the prepared undoped and Er_2O_3 doped TeO_2 glasses are characterized by two broad envelopes cover the range from 250 to 550 cm^{-1} and from 620 to 1000 cm^{-1}. These two envelops could be deconvoluted to 4 centers around 450, 650, 720 and 980 cm^{-1}. The first center that is found around 450 cm^{-1} is assigned to bending and stretching vibrations of Te-O-Te linkages that are affected with the added modifier [30- 32]. The Raman band around 650 cm^{-1} could be assigned to asymmetric stretching vibrations of TeO_4 units [30, 33, 34]. The third deconvoluted center that is found around 720-770 is assigned to symmetric and asymmetric stretching modes of TeO_3 [30, 31]. While the Raman center around 980-1100 is assigned to symmetric and asymmetric stretching fundamental of PO_4 tetrahedral groups [35]. The edge at low frequency < 200cm^{-1} is due to the Boson peak which confirms the glassy structure. It shifts depending on the glass composition because of the change in the density of vibrational states [36, 37]. To reach charge neutrality condition, when TeO2 glass is doped with rare-earth ions, REs ions are incorporated at non bridging anion bonds and this shifts Boson peak to lower frequency [38]. Incorporation of WO_3 into TeO_2 glass network leads to the formation of W–O–W and Te–O–W linkages, it is known that W and Te ions have approximately the same electronegativity values, but W ions possess a higher electronic polarizability than Te ions and W–O bond is stronger than Te–O bond so formation of Te–O–W bridging bonds increases the connectivity of the glass network [39, 40]. At low concentration of WO_3, W atoms participate in the glass network as WO_4 that reaches its maximum value at 30 mol% while at higher concentrations W atoms are incorporated

as WO_6 that is characterized by the peak around 350 cm^{-1} [41, 42], In our prepared WO_3-modified TeO_2 glass sample the peak around 350 that is assigned to bending vibrations in W-O-W in WO_6 units is absent as this sample contains low concentration of WO_3 that results in the peaks around 450 cm^{-1} that is assigned to Te-O-W stretching vibrations indicating substitution of TeO_4 by WO_4 tetrahedral units. Also, the peak at 920 cm^{-1} is characteristic of asymmetric vibrations of WO_4 tetrahedra [43]. For Al_2O_3 modified TeO_2 glass sample, suggesting a similar transformation of the tetrahedral Te$_4$ units to Te$_3$ units also due to the larger number of oxygen atoms introduced when compared to MO modified glasses. The low-frequency peak at $\approx$ 460 cm^{-1} is enhanced due to the formation of Te-O-Al bridges as their bending contributed to this band [44].
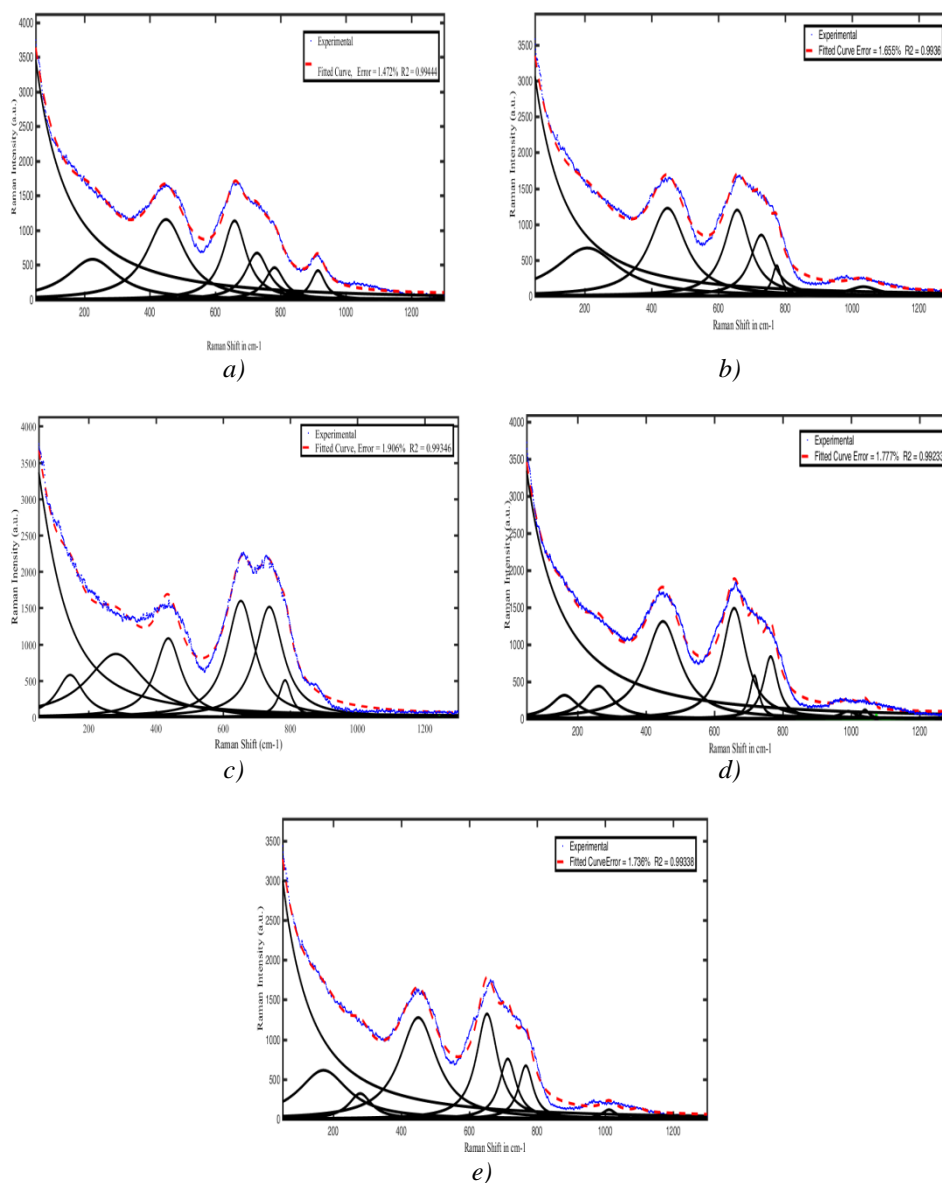

Fig. 1 Raman spectra of prepared glasses: a) WO₃; b) CdO; c) Al₂O₃; d) SrO; e) BaO

Because of similar bond strength of the dissolution of Al-O and Te-O, Al_2O_3 could cross-link strongly the glass network by Te-O-Al bridges. The band observed also around 805 is attributed to the Al-O linkages [44]. The conversion of $TeO_4 \rightarrow TeO_3$ by the addition of divalent cation and high basicity oxygen anion is confirmed in many reports of MO–TeO_2 glasses Raman spectra [46-48]. The introduction of ZnO or divalent alkaline-earth ion (M^{2+}) and oxygen anions having high basicity affects the connection of Te-O-Te and leads to the termination of Te–O- with

M^{2+} ions. Finally, TeO_4 units are converted to a TeO_3 with a terminating double bond of Te=O [46]. The deconvoluted data also show that with increasing the electronegativity, the center around 650 cm^{-1}, shifts toward higher energy except Al_2O_3 containing glasses this center is found at lower energy position while the peak center around 720&770cm^{-1} shifts toward higher energies 738 &785 cm^{-1} in W&AL containing glasses, see fig.. also have the highest relative intensity, see fig.1.This may be due to the higher coordination of Wand Al that offers more oxygen than alkaline modifiers so it has a higher rate of transformation of Te$_4$ to Te$_3$ units.
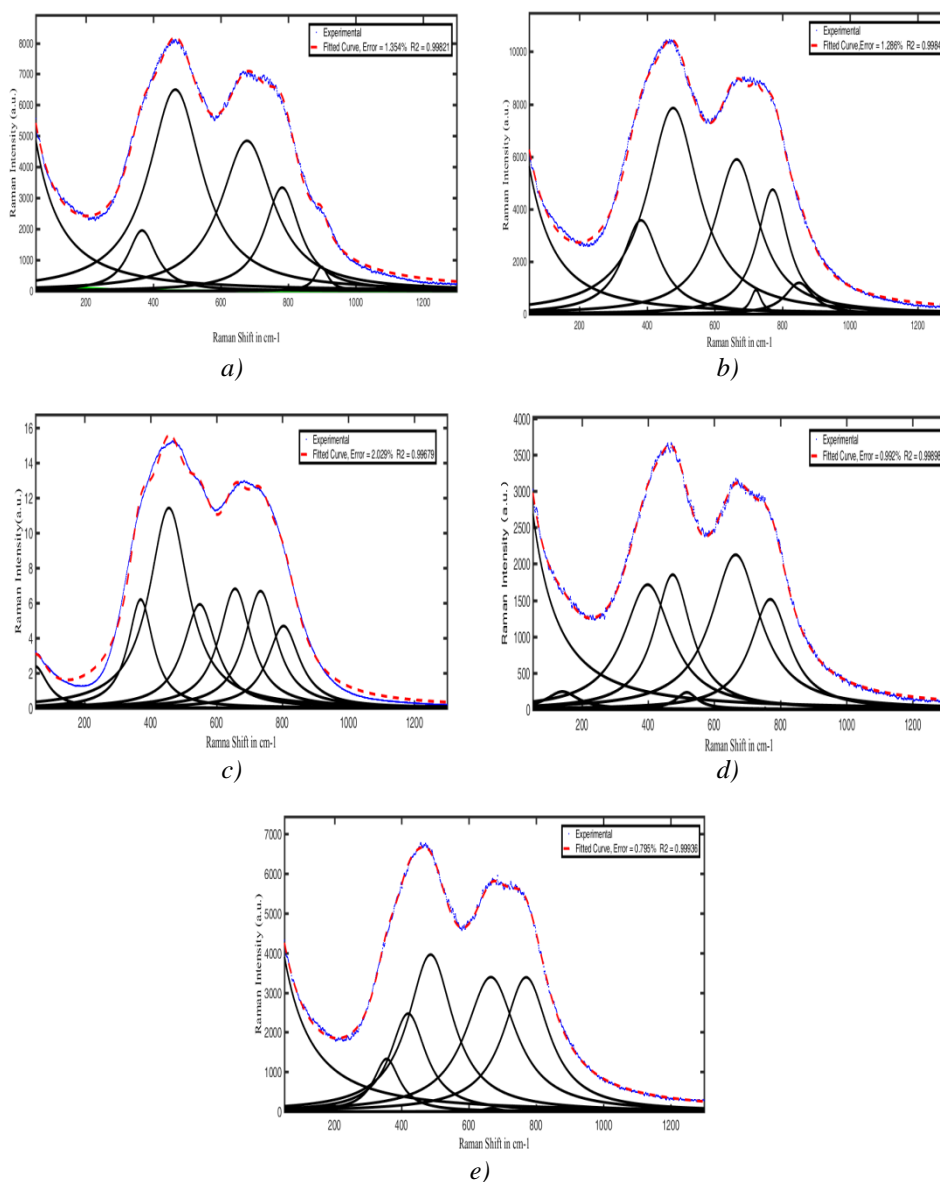

Fig. 2 Deconvolution of Raman spectra of prepared glasses.
a) WO3- Er$_2$O$_3$; b) Cd- Er$_2$O$_3$; c) Al - Er$_2$O$_3$; d) SrO- Er$_2$O$_3$; e) BaO - Er$_2$O$_3$

Doping with Er_3O_2 oxides causes a shift towards higher energy for Raman bands and especially affects the band assigned to Te-O vibrations in the (TeO_3) ($\approx$750 cm^{-1}) [49]. Also, the addition of Er^{3+} shows a band at about 350 cm^{-1} that is attributed to deformed Te-O-Te linkages in the glass network [49, 50]. The area of the band assigned to TeO_4 groups decreases for the benefit of the band assigned to TeO_3, especially in Al-modified glasses, see Fig. 3. An increase of relative intensity of the band assigned to TeO_3

vibrations after doping is also observed, which confirms the conversion of TeO_4 units into TeO_{3+1}/TeO_3 units through the formation of NBOs [51].
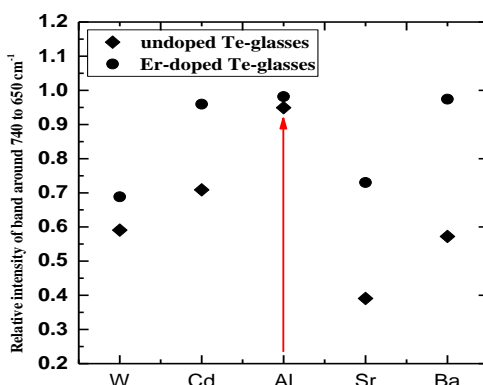

Fig. 3. Relative intensity of band at range 650 to 740nm with different modifier.

The Raman gain coefficient of the prepared glasses can be calculated using the following equations [52- 54]:

$$g_{sam}(\upsilon) = I_{corr.}(\upsilon) \times g_{SiO_2} \times \left[\frac{n_{si}(\upsilon_1 - \upsilon_p)}{n_{sam}(\upsilon_1 - \upsilon)}\right]^2 \times \left[\frac{(\upsilon_1 - \upsilon_p)}{(\upsilon_1 - \upsilon)}\right]^3 \quad (1)$$

$$I_{corr.}(\upsilon) = I_{meas.}(\upsilon).F_R(\upsilon).F_A(\upsilon).\frac{1}{F_{BE}(\upsilon,T)+1} \quad (2)$$

$$I_{meas.} \rightarrow \text{measured intensity } F_R(\upsilon) = \frac{(1+n_{sam})^4.(n_{Si})^2}{(1+n_{Si})^4.(n_{Sam})^2} \quad (3)$$

$$F_A(\upsilon) = \frac{(n_{Sam})^2}{(n_{Si})^2} \quad (4)$$

$$F_{BE}(\upsilon, T) = \frac{1}{\exp\left(\frac{hc}{K_B T}\right) - 1} \quad (5)$$

where: h is plank`s constant, C is speed of light, K_B is Boltzman constant, T is the temperature of Raman Experiment, g_{SiO2} is Raman peak gain of silica which is 1.85×10^{-13} mW^{-1} at λ= 532 nm pumping. υ is Raman shift frequency relative to pump wavelength $\upsilon_1 = 1.88 \times 10^4$ cm^{-1} , $\upsilon_p =$ 440 cm^{-1}. The values of refractive index of for WO_3 and CdO modified glasses are obtained directly from the reference [55] while for Al_2O_3, SrO and BaO modified glasses, refractive index was calculated from the values of the Energy band gap using the following equation [56]:

$$\left(\frac{n^2 - 1}{n^2 + 2}\right) = 1 - \left(\frac{E_{opt}}{20}\right)^{1/2} \quad (6)$$

E_{opt} was calculated using UV-Vis spectra from previous work ref.[57] using the model proposed by Davis and Mott [58]:

$$\alpha(\upsilon) = \frac{A(h\upsilon - E_{opt})^n}{h\upsilon} \quad (7)$$

where A is an energy-independent constant, E_{opt} is the optical band gap and n is a constant which determines the type of the optical transition.[n=1/2: direct allowed transition, n=2: Indirect allowed transition, n=1/3: direct forbidden transition, n=3: indirect forbidden transition], see Table 1.

Table. 1. Glasses composition, optical energy gap, and refractive index of prepared glasses.

Sample Code	Composition	Eopt	n	Ref
W	$70TeO_2–5WO_3–10P_2O_5–10ZnO–5PbF_2$	3.03	2.14	55
W-Er	$70TeO_2–5WO_3–10P_2O_5–10ZnO–5PbF_2$+ 600ppm Er_2O_3	3.01	2.17	55
Cd	$70TeO_2–5CdO–10P_2O_5–10ZnO–5PbF_2$	3.41	2.20	55
Cd-Er	$70TeO_2–5CdO–10P_2O_5–10ZnO–5PbF_2$ + 600ppm Er_2O_3	3.34	2.44	55
Al	$70TeO_2–5Al_2O_3–10P_2O_5–10ZnO–5PbF_2$	2.85	2.44	57
Al-Er	$70TeO_2–5Al_2O_3–10P_2O_5–10ZnO–5PbF_2$ + 600ppm Er_2O_3	2.80	2.45	57
Sr	$70TeO_2–5SrO–10P_2O_5–10ZnO–5PbF_2$	2.84	2.44	57
Sr-Er	$70TeO_2–5SrO–10P_2O_5–10ZnO–5PbF_2$ + 600ppm Er_2O_3	2.885	2.429	57
Ba	$70TeO_2–5BaO–10P_2O_5–10ZnO–5PbF_2$	2.833	2.444	57
Ba-Er	$70TeO_2–5BaO–10P_2O_5–10ZnO–5PbF_2$ + 600ppm Er_2O_3	2.89	2.427	57

The Raman gain peak is found at about 675 cm^{-1}, see Fig.4a,b,c,d. for examples. The obtained value for the Raman gain coefficient of the prepared glasses is ranging from 6.34x10^{-12} to 5x10^{-10} m/W. All the prepared glasses have a higher Raman gain coefficient than that is reported for silica (1.85×10^{-13} mW^{-1}), see Table 2. Al_2O_3 modified glasses have the highest Raman gain coefficient. It can be noticed also that doping with Er_2O_3 increases the Raman gain coefficient for the prepared glasses with Al2O3 modified glass sample has the highest Raman gain coefficient. The Raman gain coefficient of the prepared glasses was compared also with other glass systems, see Table 2.
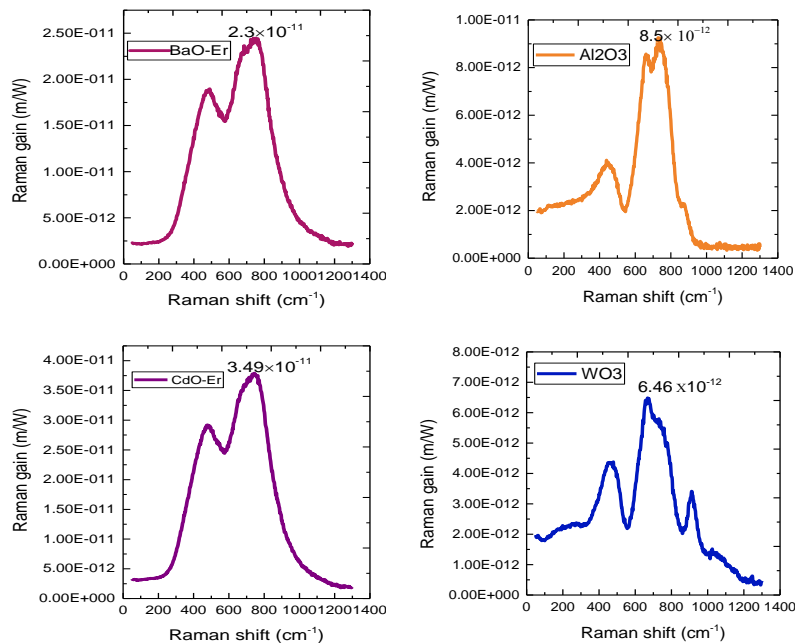

Fig. Raman gain coefficient of prepared glasses.

Table 2. The Raman gain coefficient of prepared glasses.

Sample Code	Composition	Gain m/W	Ref.
W	$70TeO_2–5WO_3–10P_2O_5–10ZnO–5PbF_2$	6.46×10^{-12}	Present work
W-Er	$70TeO_2–5WO_3–10P_2O_5–10ZnO–5PbF_2+ 600ppm\ Er_2O_3$	2.76×10^{-11}	Present work
Cd	$70TeO_2–5CdO–10P_2O_5–10ZnO–5PbF_2$	6.34×10^{-12}	Present work
Cd-Er	$70TeO_2–5CdO–10P_2O_5–10ZnO–5PbF_2 + 600ppm\ Er_2O_3$	3.49×10^{-11}	Present work
Al	$70TeO_2–5Al_2O_3–10P_2O_5–10ZnO–5PbF_2$	8.5×10^{-12}	Present work
Al-Er	$70TeO_2–5Al_2O_3–10P_2O_5–10ZnO–5PbF_2 + 600ppm\ Er_2O_3$	5×10^{-10}	Present work
Sr	$70TeO_2–5SrO–10P_2O_5–10ZnO–5PbF_2$	6.65×10^{-12}	Present work
Sr-Er	$70TeO_2–5SrO–10P_2O_5–10ZnO–5PbF_2 + 600ppm\ Er_2O_3$	1.23×10^{-11}	Present work
Ba	$70TeO_2–5BaO–10P_2O_5–10ZnO–5PbF_2$	6.66×10^{-12}	Present work
Ba-Er	$70TeO_2–5BaO–10P_2O_5–10ZnO–5PbF_2 + 600ppm\ Er_2O_3$	2.3×10^{-11}	Present work
	$80TeO_2–10Na_2O–10ZnO$ $90TeO_2–5WO_3–5Nb_2O_5$ $70TeO_2–25WO_3–5Bi_2O_3$	19.9×10^{-13} 29.7×10^{-13} 23.9×10^{-13}	[2]
	$75TeO_2-5WO_3-15Nb_2O_5-5CuO$ $75TeO_2-5WO_3-15Nb_2O_5-5Na_2O$	0.14×10^{-12} 4.43×10^{-12}	[35]
	$77TeO_2–10Na_2O–10ZnO–3PbO$ $65TeO_2–10Na_2O–25ZnF_2$ $50TeO_2–50TlO$ $85TeO_2–15WO_3$	17×10^{-13} 7.5×10^{-13} 52×10^{-13} 38×10^{-13}	[36]

4. Conclusions

The glass composition affects the Amplitude and the energy of the Boson peak. The transformation of Te_4 to Te_3 is more obvious in Al_2O_3 modified glass sample. Raman bands also shift to higher energy after doping while Boson peak shifts to lower frequency to satisfy the neutrality condition. As W-O bond is stronger than Te-O bond, Addition of WO_3 increases the connectivity of the glass network due to the formation of Te–O–W bridging bonds.

Al_2O_3 could cross-link strongly the glass network by Te-O-Al bridges. ZnO or/and divalent alkaline-earth ion (M^{2+}) and oxygen anions affect the connection of Te-O-Te and lead to the termination of Te–O- with M^{2+} ions and finally, TeO_4 units are converted to a TeO_3 with a terminating double bond of Te=O. Doping with Er^{3+} ions results in the deformation of Te-O-Te linkages. Raman gain was calculated and found to increase after doping. Al_2O_3 modified glasses have the highest Raman gain

Acknowledgments

214

References

[1] A. Jha,, B. D. O. Richards, G. Jose, T. Toney Fernandez, C. J. Hill, J. Lousteau, P. Joshi, International Materials Reviews **57**(6), 357 (2012).

[2] Md. O'Donnell, K. Richardson, R. Stolen, C. Rivero, T. Cardinal, M. Couzi, D. Furniss, A. B. Seddon, Optical Materials **30**(6), 946 (2008).

[3] Feifei Chen, Tiefeng Xu, Shixun Dai, Qiuhua Nie, Xiang Shen, Jianliang Zhang, Xunsi Wang, Optical Materials **32**(9), 868 (2010).

[4] N. S. Tagiara, D. Palles, E. D. Simandiras, V. Psycharis, A. Kyritsis, E. I. Kamitsos, Journal of Non-Crystalline Solids **457**, 116 (2017).

[5] M. J. Weber, Journal of Non-Crystalline Solids **123**(1-3), 208 (1990).

[6] E. M. Vogel, M. J. Weber, D. M. Krol, Phys. Chem. Glasses **32**, 231 (1991).

[7] Honma, Tsuyoshi, Noriko Ito, Takayuki Komatsu, Vesselin Dimitrov, Journal of the American Ceramic Society **93**(10), 3223 (2010).

[8] L. A. Bueno, A. S. Gouveia-Neto, E. B Da Costa, Y. Messaddeq, S. J. L. Ribeiro, Journal of Physics: Condensed Matter **20**(14), 145201 (2008).

[9] H. A. Othman, Hagar S. Elkholy, Ibrahim Z. Hager, International Journal of Applied Glass Science **8**(3), 313 (2016).

[10] H. A. Othman, H. S. Elkholy, I. Z. Hager, Materials Research Bulletin **89**, 210 (2017).

[11] B. Afef, H. H. Hegazy, H. Algarni, Y. Yang, K. Damak, E. Yousef , R. Maâlej, J. Rare Earths **35**(4), 361 (2017).

[12] K. Damak, R. Maâlej, E. Yousef, A. Qusti, C. Rüssel, J. Non-Cryst. Solids **358**, 2974 (2012).

[13] H. A. Othman, G. M. Arzumanyan, D. Möncke, Optical Materials **62**, 689 (2016).

[14] D. Rajesh, Y. C. Ratnakaram, M. Seshadri, A. Balakrishna, T. Satya Krishna, Journal of Luminescence **132**(3), 841 (2012).

[15] H. A. Othman, H. S. Elkholy, I. Z. Hager, Journal of Molecular Structure **1106**, 286 (2016).

[16] Nirmal Kaur, Atul Khanna, Marina Gónzález-Barriuso, Fernando González, Banghao Chen, Journal of Non-Crystalline Solids **429**, 153 (2015).

[17] Kazuo Arai, Hiroshi Namikawa, Ken Kumata, Tatsutoku Honda, Yoshiro Ishii, Takashi Handa, Journal of Applied Physics **59**(10), 3430 (1986).

[18] G. Upender, Suresh Bharadwaj, A. M. Awasthi, V. Chandra Mouli, Materials Chemistry and Physics **118**(2-3), 298 (2009).

[19] G. Upender, Suresh Bharadwaj, A. M. Awasthi, V. Chandra Mouli, Materials Chemistry and Physics **118**(2-3), 298 (2009).

[20] J. S. Wang, E. M. Vogel, E. Snitzer, Optical Materials **3**(3), 187 (1994).

[21] Zhengda Pan, Steven H. Morgan, Keith Dyer, Akira Ueda, Huimin Liu, Journal of Applied Physics **79**(12), 8906 (1996).

[22] Yong Ding, Shibin Jiang, Bor-Chyuan Hwang, Tao Luo, Nasser Peyghambarian, Yusuke Himei, Tomoko Ito, Yoshinari Miura, Optical Materials **15**(2), 123 (2000).

[23] R. Rolli, M. Montagna, S. Chaussedent, A. Monteil, V. K. Tikhomirov, M. Ferrari, Optical Materials **21**(4), 743 (2003).

[24] Alexander A. Kaminskii, Annales De Physique **16**(6), 639 (1991).

[25] Elivelton Alves Ferreira, Fábia Castro Cassanjes, Gael Poirier, Optical Materials **35**(6), 1141 (2013).

[26] M. Reza Dousti, M. R. Sahar, S. K. Ghoshal, Raja J. Amjad, R. Arifin, Journal of Non-Crystalline Solids **358**(22), 2939 (2012).

[27] J. C. Liang, X. Q. Zhou, Journal of the Optical Society of America B **22**(11), 2468 (2005).

[28] Robert Stegeman, Ladislav Jankovic, Hongki Kim, Clara Rivero, George Stegeman, Kathleen Richardson, Peter Delfyett, Yu Guo, Alfons Schulte, Thierry Cardinal, Optics Letters **28**(13), 1126 (2003).

[29] P. Nandi, G. Jose, Physica B: Condensed Matter **381**(1-2), 66 (2006).

[30] Jackson, Jessica, Charmayne Smith, Jonathan Massera, Clara Rivero-Baleine, Corey Bungay, Laeticia Petit, Kathleen Richardson, Optics Express **17**(11), 9071 (2009).

[31] Kaur, Amandeep, Atul Khanna, Fernando González, Carmen Pesquera, Banghao Chen, Journal of Non-Crystalline Solids **444**, 1 (2016).

[32] I. Shaltout, Yi Tang, R. Braunstein, A. M. Abu-Elazm, Journal of Physics and Chemistry of Solids **56**(1), 141 (1995).

[33] Murugan, G. Senthil, Yasutake Ohishi, Journal of Applied Physics **96**(5), 2437 (2004)

[34] Takao Sekiya, Norio Mochida, Atsushi Ohtsuka, Journal of Non-Crystalline Solids **168**(1-2), 106 (1994).

[35] S. F. Mansour et al., Solid State Sciences **37**, 33 (2014).

[36] M. D. Odonnell et al., Journal of the American Ceramic Society **90**(5), 1448 (2007).

[37] V. K. Malinovsky, A. P. Sokolov, Solid State Communications **57**(9), 757 (1986).

[38] V. K. Tikhomirov, A. Jha, A. Perakis, E. Sarantopoulou, M. Naftaly, V. Krasteva, R. Li, A. B Seddon, Journal of Non-Crystalline Solids **256-257**, 89 (1999).

[39] Mohamed Ataalla, Ahmed S. Afify, Mohamed Hassan, Mohamed Abdallah, Margarita Milanova, Hassan Y. Aboul-Enein, Amr Mohamed, Journal of Non-Crystalline Solids **491**, 43 (2018).

[40] L. Schneebeli, K. Kieu, E. Merzlyak, J. M. Hales, A. Desimone, J. W. Perry, R. A. Norwood, N. Peyghambarian, Journal of the Optical Society of America B **30**(11), 2930 (2013).

[41] G. Upender, Suresh Bharadwaj, A. M. Awasthi, V. Chandra Mouli, Materials Chemistry and Physics **118**(2-3), 298 (2009).

[42] B. V. R. Chowdari, P. Pramoda Kumari, Solid State Ionics **86-88**, 521 (1996).

[43] V. O. Sokolov, V. G. Plotnichenko, V. V. Koltashev, E. M. Dianov, Journal of Non-Crystalline Solids **352**(52-54), 5618 (2006).

[44] Amandeep Kaur, Atul Khanna, Marina González-Barriuso, Fernando González, Banghao Chen, Journal of Non-Crystalline Solids **470**, 14 (2017).

[45] K. Maheshvaran, P. K. Veeran, K. Marimuthu, Solid State Sciences **17**, 54 (2013)

[46] Tomokatsu Hayakawa, Masahiko Hayakawa, Masayuki Nogami, Philippe Thomas, Optical Materials **32**(3), 448 (2010).

[47] Takao Sekiya, Norio Mochida, Atsushi Ohtsuka, Journal of Non-Crystalline Solids 168(1-2), 106 (1994).

[48] Jong Heo, David Lam, George H. Sigel, Edgar A. Mendoza, David A. Hensley, Journal of the American Ceramic Society **75**(2), 277 (1992).

[49] Amarjot Kaur, Atul Khanna, Lyubomir I. Aleksandrov, Journal of Non-Crystalline Solids **476**, 67 (2017).

[50] N. Jaba, A. Mermet, E. Duval, B. Champagnon, Journal of Non-Crystalline Solids **351**(10-11), 833 (2005).

[51] Katarzyna Pach, Edmund Golis, El Sayed Yousef, Maciej Sitarz, Jacek Filipecki, Journal of Molecular Structure **1164**, 328 (2018).

[52] El Sayed Yousef, H. H. Hegazy, Samar Almojadah, M. Reben, Optics & Laser Technology **74**, 138 (2015).

[53] Takenobu Suzuki, Teruo William Shiosaka, Shohei Miyoshi, Yasutake Ohishi, Journal of Non-Crystalline Solids **357**(14), 2702 (2011).

[54] R. H. Stolen, E. P. Ippen, Applied Physics Letters **22**(6), 276 (1973).

[55] R. Miedzinski, I. Fuks-Janczarek, M. Reben, Y. El Sayed Said, Optical Materials **85**, 48 (2018).

[56] Vesselin Dimitrov, Sumio Sakka, Journal of Applied Physics **79**(3), 1736 (1996).

[57] M. Reben, El. Sayed Yousef, M. Piasecki, A. A. Albassam, A. M. El-Naggar, G. Lakshminarayana, I. V. Kityk, I. Grelowska, Journal of Materials Science: Materials in Electronics **28**(12), 8969 (2017).

[58] E. A. Davis, N. F. Mott, Philosophical Magazine **22**(179), 0903 (1970).